Article:
Ali, H., Ma, L., Ghadbeigi, H. et al. (1 more author) (2017) In-situ residual stress reduction, martensitic decomposition and mechanical properties enhancement through high temperature powder bed pre-heating of Selective Laser Melted Ti6Al4V. Materials Science and Engineering: A, 695. pp. 211-220. ISSN 0921-5093

https://doi.org/10.1016/j.msea.2017.04.033

In-situ residual stress reduction, martensitic decomposition and mechanical properties enhancement through high temperature powder bed pre-heating of Selective Laser Melted Ti6Al4V

Haider Ali[a], Le Ma[b], Hassan Ghadbeigi[a], Kamran Mumtaz[a]

[a] *Department of Mechanical Engineering, University of Sheffield, Sheffield, UK*

[b] *Department of Materials Science and Engineering, University of Sheffield, Sheffield, UK*

Abstract:

During the Selective Laser Melting (SLM) process large temperature gradients can form, generating a mismatch in elastic deformation that can lead to high levels of residual stress within the additively manufactured metallic structure. Rapid melt pool solidification causes SLM processed Ti6Al4V to form a martensitic microstructure with a ductility generally lower than a hot working equivalent. Post-process heat treatments can be applied to SLM components to remove in-built residual stress and improve ductility.

The use of high temperature pre-heating during an SLM build can assist in reducing thermal gradients, enable a more controlled cooling with the possibility to control/tailor as-built mechanical properties. In this work a high temperature SLM powder bed capable of pre-heating to 800ºC is used during processing of Ti6Al4V feedstock. The effect of powder bed temperature on residual stress formation, microstructure and mechanical properties was investigated. It was found that increasing the bed temperature to 570ºC significantly reduced residual stress formation within components and enhanced yield strength and ductility. This pre-heating temperature enabled the decomposition of α' martensitic microstructure into an equilibrium α+β microstructure. At 570ºC the yield strength and elongation of components was improved by 3.2% and 66.2% respectively.

Keywords

Ti6Al4V, Selective Laser Melting, Additive Manufacturing, Mechanical Properties, Residual Stress, Powder Bed Pre-Heating.

1 Introduction

Additive Manufacturing (AM) techniques are capable of fabricating fully functional three dimensional parts from a digital model by joining material in a layer by layer process [1, 2]. Direct production of parts without the requirement for specific tooling enhances the geometric freedom of the process enabling the manufacture of complex geometries, which can reduce production time and cost of production for one-off customised geometries [2]. Selective Laser Melting (SLM) is an AM process in which metallic powder is selectively melted and fused by a high powered laser to create high density components. Cross-sections of the part are fused in layers, which are built up successively to create the complete 3D object. The method of layered fabrication, combined with the high precision of laser melting allows for a greatly expanded design freedom with minimal feedstock waste. The technology is greatly applicable for use in high value markets such as the aerospace industry and in particular for use of high performance materials such as titanium-based alloys. The characteristic properties of these alloys (increased hardness and tensile strength) can make them difficult to form using conventional techniques [3]. A significant problem associated with components manufactured using SLM is the development of high internal residual stresses [3]. Rapid heating and cooling cycles of successive layers of powder feedstock generates large temperature gradients during a component build. If residual stresses are not considered during the part design and build setup, they can contribute to the failure of a component during an SLM build or later in service, particularly one subjected to alternating loadings or corrosive environments [3-14]. Often some form of post-processing heat treatment cycle are applied to SLM components to relieve residual stresses and generate the required mechanical properties. This requirement for post-processing operations can substantially increase manufacturing time and cost of SLM components [15]. Most commercially available SLM systems offer low temperature powder bed pre-heating as an option to reduce thermal gradients during processing and improve powder flow by removing any moisture

within the powder/chamber. However pre-heating temperatures within commercial SLM systems are generally limited to below 200ºC due to machine design and challenges associated with operation at significantly higher temperatures. Investigations that have used high pre-heating temperature have often been custom modified by investigators. The highest SLM bed pre-heat temperature reported in published literature is 400ºC, in the work by Vracken et al [16]. It is reported that SLM formed components possess lower ductility compared with the hot worked materials [17-19]. Additionally, the thermally induced residual stresses generated within the process may lead to cracking within components [20]. Process-induced defects such as the presence of internal pores, may increase the stress concentration locally and lead to early failure and lower ductility [21].

Ti6Al4V is an α+β alloy, which has higher strength compared to α alloys, and a wider processing window as compared to both α and β alloys [22]. Ti6Al4V possesses a low density and high strength at low to moderate temperatures, being widely used in aerospace, automotive and medical sectors [23]. α+β alloys transform martensitically if the cooling rate from the β field to room temperature is high [24]. SLM Ti6Al4V primarily form a microstructure containing mainly acicular martensite that leads to high strength and low ductility [25]. SLM fabricated components with high density characteristically attain a high yield strength, but limited ductility due to the martensitic microstructure. The martensitic microstructure is formed due to the high cooling rates inherent in the SLM process. Transforming the martensite into α+β microstructure results in improved ductility and reduced internal residual stresses [25]. The martensitic decomposition temperature for Ti6Al4V is 600-650ºC [18, 26, 27]. The annealing temperature ranges from 700-790ºC [23]. Studies that have focused on reducing residual stress during an SLM build have found pre-heating of the powder bed to be the most effective in-situ stress reduction method [5, 13, 16, 28, 29]. However, there is no consensus on the optimal temperature required to get the best results for the SLM process (also considering resultant mechanical properties). The optimum range of bed pre-heat temperature for a combination of minimum residual stress and acceptable mechanical properties is yet to be established. Various post-process heat

treatment cycles have also been used to reduce internal residual stress as well as improve the ductility of SLM parts [29-31]. However, due to the distinctively fine dendritic microstructure formed within SLM parts, the applied conventional heat treatment strategies do not always produce the desired results [30].

SLM processing Ti6Al4V at higher powder bed pre-heat temperature will serve a dual purpose, first by facilitating in-situ martensitic decomposition (as well as annealing which may result in SLM parts with higher ductility) and secondly reducing residual stresses (as is obtained during the customary high temperature powder bed pre-heating during electron beam melting).

The objective of this work was to investigate the effect of high temperature powder bed pre-heating on residual stress, microstructure and mechanical properties of SLM Ti6Al4V parts.

2 Experimental methodology and testing

2.1 SLM build setup and elevated powder bed pre-heating

This investigation used a Renishaw SLM125 system for Ti6Al4V density optimisation trials, fabrication of residual stress blocks and tensile samples using variable pre-heat temperatures. The SLM125 uses a 200W fiber laser and has a standard build volume of 125x125x125mm, a schematic of Renishaw SLM 125 is shown in Figure-1(a). A modified pre-heating platform is shown in Figure-1(b), was designed and integrated into the SLM125 system, enabling controlled powder bed heating up to 800ºC. Conductive controlled heating elements were used to maintain a constant temperature at a set level throughout the build process. Due to the requirement for increased thermal insulation within the build chamber, the platform build area was reduced to 66x66mm. Using the elevated pre-heating capability, samples were manufactured at 370ºC, 470ºC, 570ºC, 670ºC and 770ºC. Three of the selected temperatures are related to specific microstructural transformation limits for Ti6Al4V. 570ºC is 30ºC below the lower limit of the martensitic decomposition temperature range of 600-670ºC for Ti6Al4V. 670ºC is the higher limit for the martensitic decomposition temperature range and 30ºC below the lower limit for

the annealing temperature range of 700-790ºC for Ti6Al4V. 770ºC is 20ºC below the higher limit of the annealing temperature range.

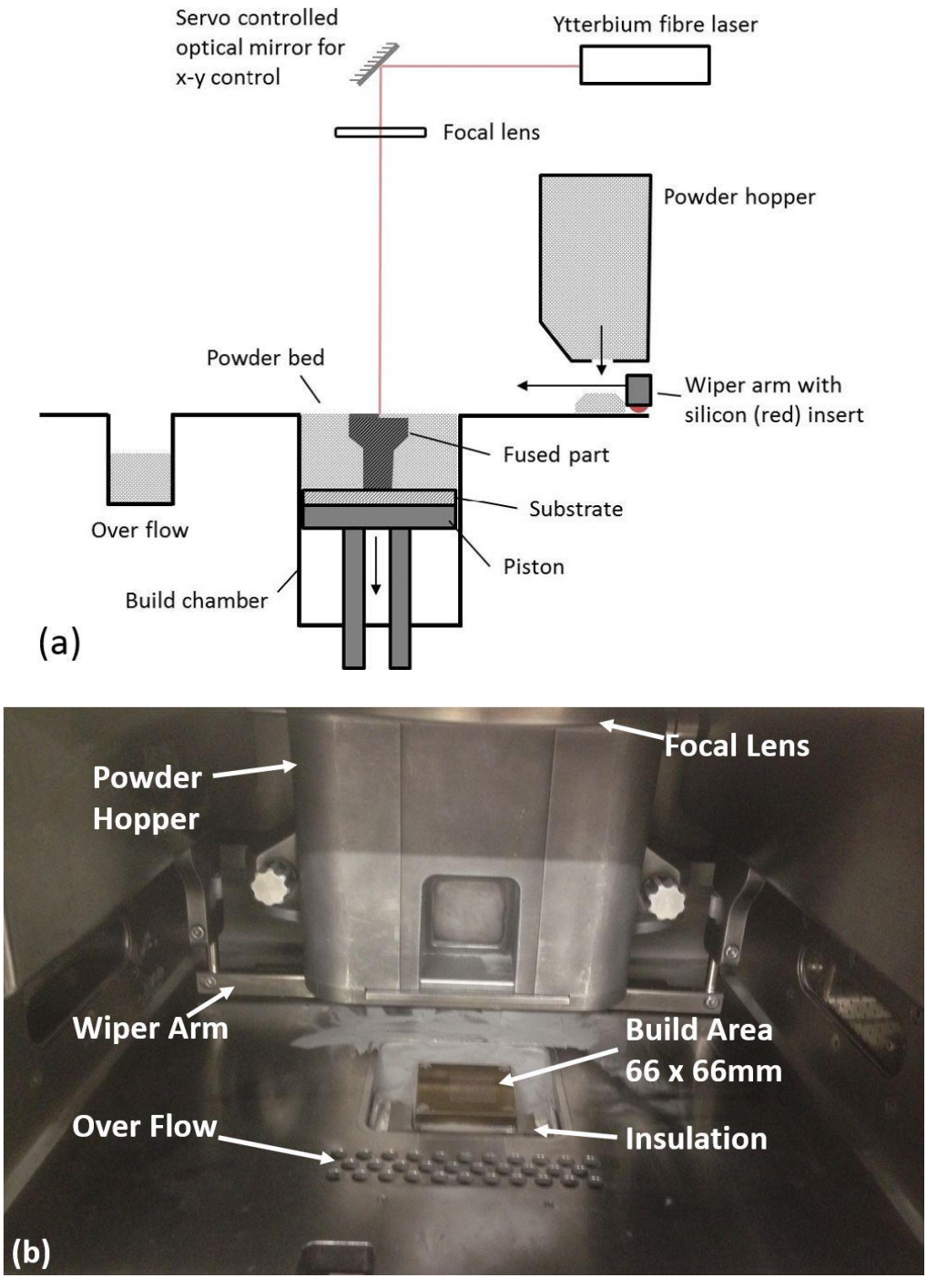

Figure 1 (a) Schematic of the SLM build process for Renishaw SLM 125 [32].

(b) Renishaw SLM 125 system chamber with custom designed heated bed

2.2 **Material and processing parameters**

Ti6Al4V-ELI powder with a particle size of 15-45µm from Technik Spezialpulver (TLS), was used within this investigation. 10X10X10mm blocks were manufactured at 100ºC powder bed pre-heat temperature for density optimisation trials. These trials were undertaken using the default Ti64 Renishaw SLM parameters (laser focus offset 0, hatch spacing 0.08mm, contour spacing 0.2, layer thickness 50µm, scanning strategy 90º alternative). Laser power and exposure time was varied between 120-200W and 60-180µs respectively. Table-1 shows the different test cases designed for powder bed pre-heating.

Table 1. Test cases based on bed pre-heat temperature

Case Number	T1	T2	T3	T4	T5	T6
Bed Pre-Heat Temperature (^{o}C)	100	370	470	570	670	770

2.3 **Density and microstructural testing**

Area fraction analysis of representative micrographs/fields using a method based on ASTM E2109-01 (2007) and BS 7590:1992[33, 34] was used to estimate the volume fraction of porosity in cube samples. The apparent contrast under a microscope was used to differentiate porosity from its surroundings and subsequent thresholding of grey values was used to exclude all non-porosity constituents in the micrographs/live image. Samples were cross sectioned perpendicular to build direction, mounted and prepared for optical and Scanning Electron Microscopy (SEM). Mounted samples were etched using Kroll's (92 ml distilled water, 6 ml Nitric Acid and 3 ml Hydrofluoric Acid) agent. The etched surface of the samples was analysed using Olympus BX60 optical microscope and images were taken at 5X to 200X magnification for microstructural analysis. Inspect F50 high resolution Field Emission Scanning Electron Microscope (FEG-SEM) was used to reveal the microstructural morphology and features of interest at higher magnifications.

2.4 **Mechanical properties and residual stress measurements**

Three tensile test specimens were manufactured for each bed pre-heat temperature case, according to ASTM- E8 / E8M-13a standard [35]. The specimens were tested at a crossheads displacement rate of $0.5\frac{mm}{min}$ on an Instron 5567B723 with clip-on extensometers using BS EN ISO6892-1 standard [36], to determine stress-strain curves of samples built under each test condition. Vickers micro hardness tests were conducted according to B EN ISO 6507-1:2005[37] using a 200g load on a Zwick Microhardness Tester. An average hardness value was calculated for each sample using 12 indentations taken along the build direction of the 30x30x10mm block cross section. Three 30x30x10mm blocks to be used for residual stress measurement, were manufactured for each bed pre-heat temperature case. Residual stress was measured on the top surface of 30x30x10mm SLM blocks. Air-abrasive hole drilling using ASTM E837-13a was used for residual stress measurement at a depth of 2mm into the sample with an average error of 5–20%. This is a semi-destructive method capable of measuring bi-axial normal (σ_{xx}, σ_{yy}) and shear (τ_{xy}) stresses [38].

3 Results and Discussion

3.1 **SLM parameter optimisation for Ti6Al4V**

Optical micrographs of Ti6Al4V SLM samples processed at variable laser powers and exposure times are shown in Figure-2. The optical micrographs indicate that the highest density is achieved in samples built with 200W laser power and a 100µs exposure time, generating components with minimum defects and density of 99.99%. The major diagonal within Figure-2, shows clear trends in the level and morphology of porosity in samples produced with varying power and exposure combination. It can be seen that the top left corner of Figure-2 represents a region of low power and low exposure creating irregular shaped pores, characteristic of lack of fusion due to insufficient energy for melting. The bottom right corner of Figure-2 represents a region of high power and high exposure creating spherical porosity. This is characteristic of over

melting due to excess heat input and potential initiation of key-hole type melting (deep melt penetration as material vaporises).

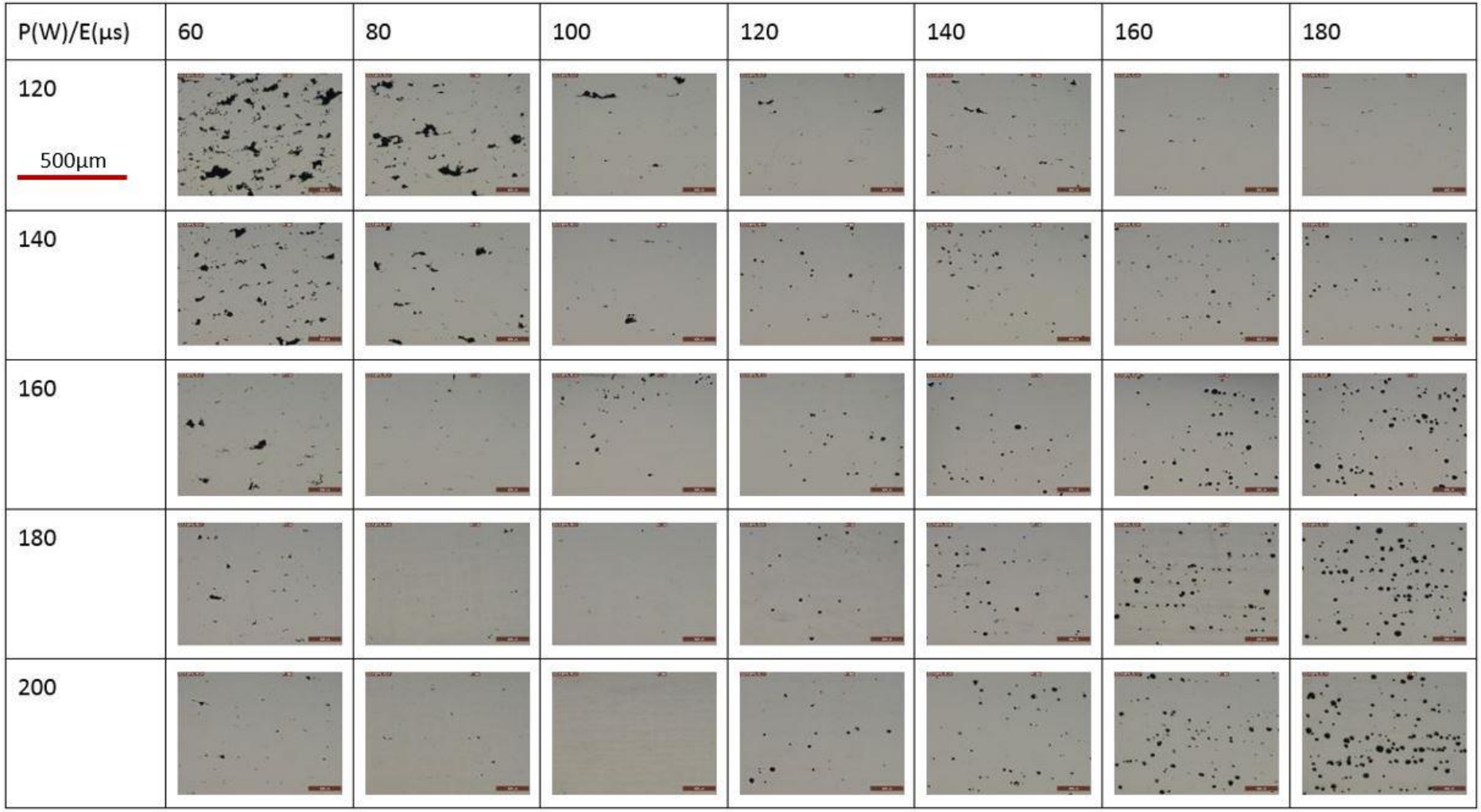

Figure-2. SLM Ti6Al4V density optimisation trials

3.2 **Microstructure**

Figure-3(a) shows the optical micrograph of case-T1 built at 100ºC bed temperature. Case-T1 has SLM Ti6Al4V characteristic martensitic α' laths within long prior columnar β grains, extending over multiple layers. Case-T1, displays completely martensitic microstructure. Figure-3(b) shows the optical micrograph of case-T6 built at 770ºC, the highest bed pre-heat temperature used in this study. Prior β grains are present even in samples built at highest bed temperature. Figure-3 shows that irrespective of the bed temperature, prior β grains characteristic of SLM Ti6Al4V are present in all samples.

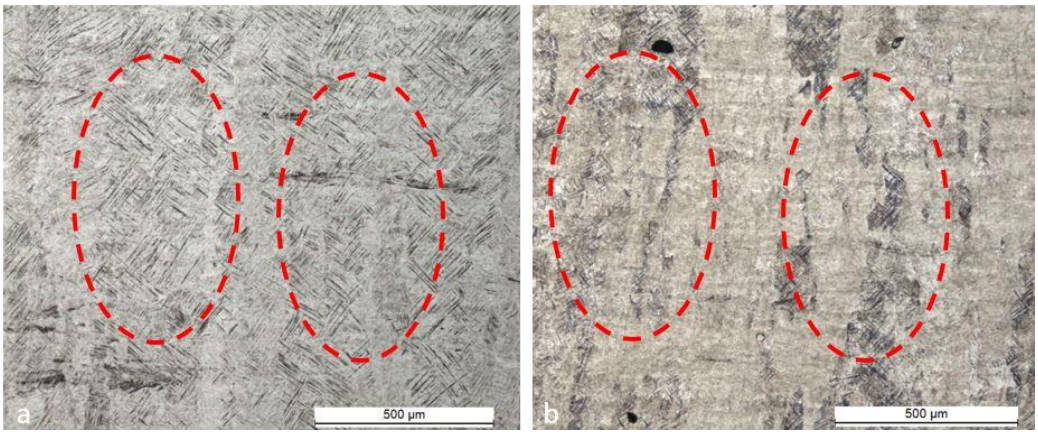

Figure-3. (a) Case-T1 (100ºC) displaying prior β columnar grains. (b) Case-T6 displaying prior β columnar grains (770ºC).

The microstructure of the samples in Case T1 (100ºC) and T2 (370ºC) are shown in Figure-4 where the optical micrographs (a) and (c) show that the microstructure remains martensitic for both the samples. Higher magnification SEM micrographs Figure-4(b) and (d) reveal that the lath size has increased as shown by the dashed ellipse and small amounts of white β particles the have formed between the α' laths (indicated with arrows), for Case-T2 some α' may have transformed into equilibrium α.

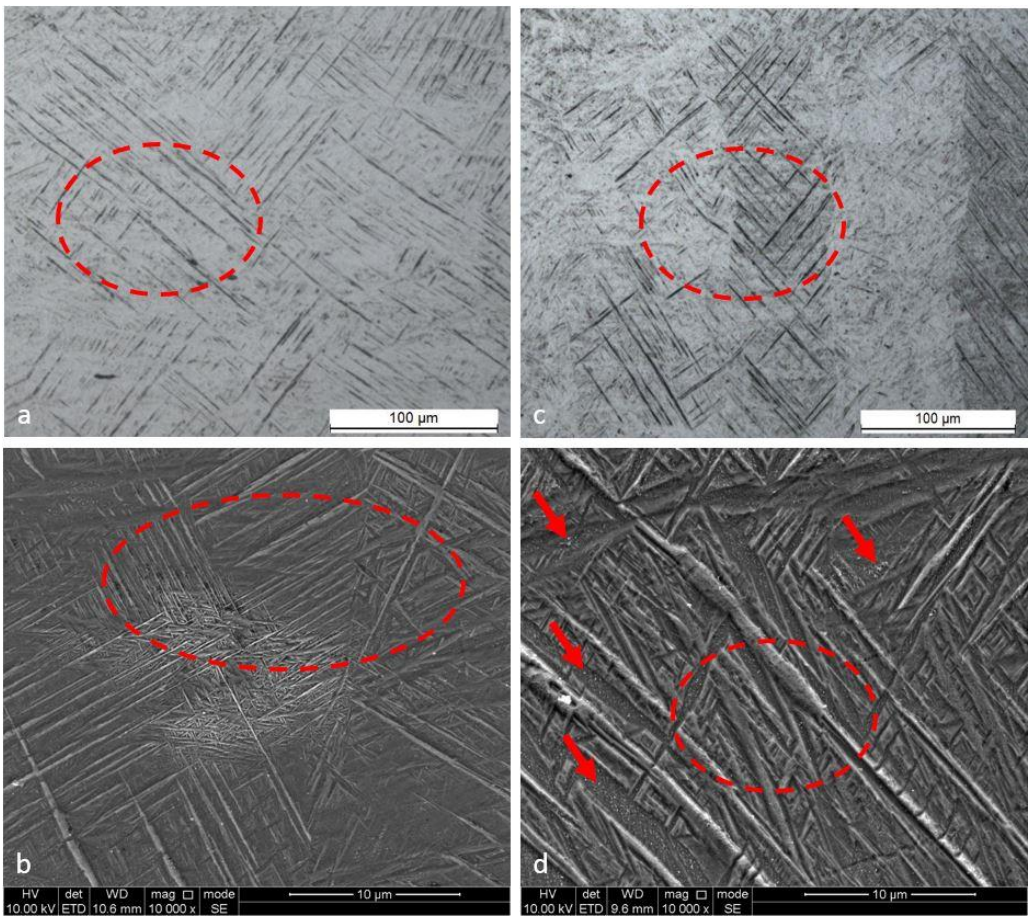

Figure-4 Martensitic microstructure of the samples in (a) Case-T1 (100ºC) with (b) showing different α' lath sizes (c) α' laths in prior β grains in Case T2 (370ºC). (d) Case-T2 shows growth in α' laths size (ellipse) and white β particles starting to form between α' laths shown by the arrows.

According to Figure-5(a), for Case-T3 (470ºC) the microstructure remains martensitic but with a considerable α' decomposition into equilibrium α as highlighted by the red circles. The SEM images in Figure-5(b), Case-T3 shows that the lath size has increased and the amount of β between the α'/α laths has increased compared to Case-T2 (370ºC) samples. The martensitic decomposition of Ti6Al4V is in the range of 600-650ºC and the selected upper limit temperature of 570ºC for Case-T4 is just below this value. However, Figure-5(c) shows that for the samples built at 570ºC there is no martensitic phase present within the sample. The sample contains a basket weave microstructure with α colonies (highlighted by red circles) and grain boundary β (as shown by arrows in Figure-5(d)) between the colonies. Figure-5(d), shows that the lath size has increased compared to samples produced at lower bed

temperatures and the amount of β between α laths has increased considerably. Another interesting feature is the formation of nano β inside α laths. Case-T5 (670ºC) in Figure-6(a) shows an increase in α lath size and marks the start of grain boundary α globulorisation. Figure-6(b) shows an increase in white β particles between α laths as well as an increase in nano β particles growing inside α laths. For the samples built at 770ºC, Figure-6(c) shows a further increase in α lath size and globular grain boundary α. Figure-6(d) shows an increase in white β particles between α laths, as well as an increase in the nano β particles growing inside α laths, as highlighted by the red arrows. According to the results shown in Figure-6 an increase in the powder bed pre-heat temperature (670ºC and 770ºC) leads to increase in α lath and colony size. The amount of the β phase growing between α lath colonies as well as nano β particles growth inside α laths has increased with increasing temperature.

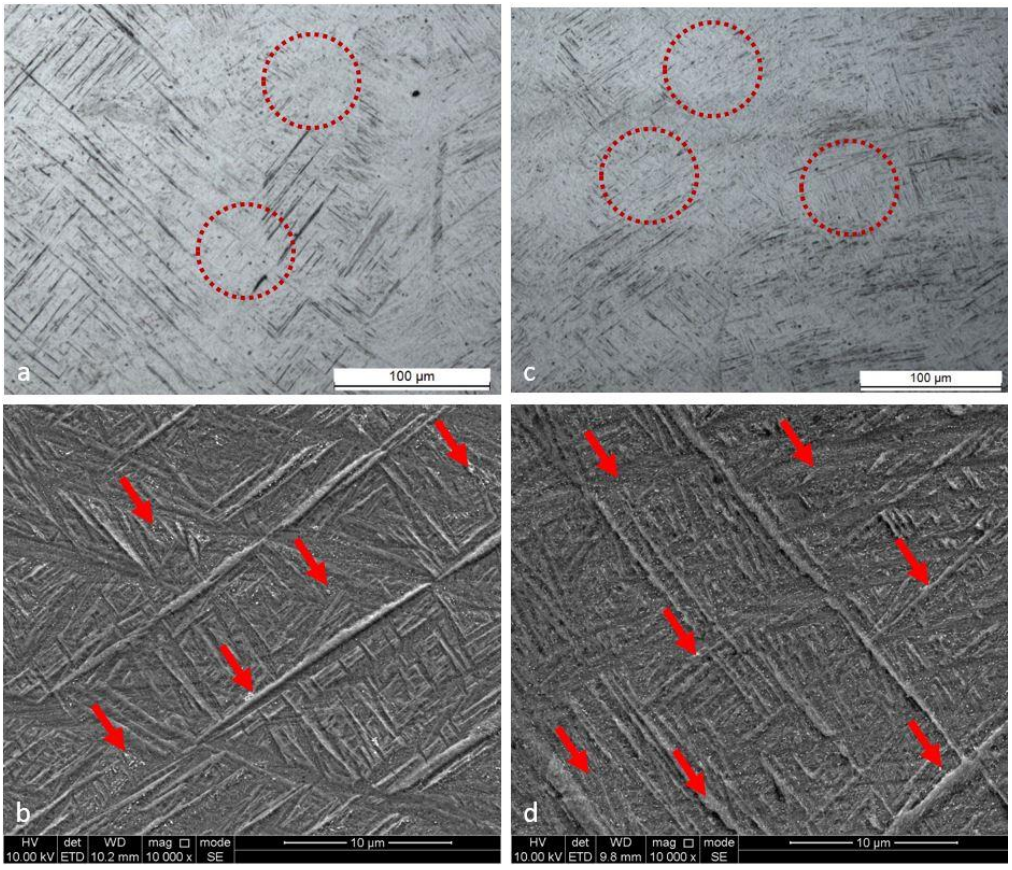

Figure-5. (a) Case-T3 (470ºC) shows decreases in α' martensitic laths due to decomposition into α, highlighted by red circles. (b) Case-T3, shows white β particles growing between α/α' laths (indicated by the arrows). (c) Case-T4 (570ºC) shows α'martensite has decomposed into equilibrium basketweave α+β microstructure,

highlighted by solid red circles. (d) Case-T4 shows β growing between α laths and β starting to grow inside α laths (indicated by arrows).

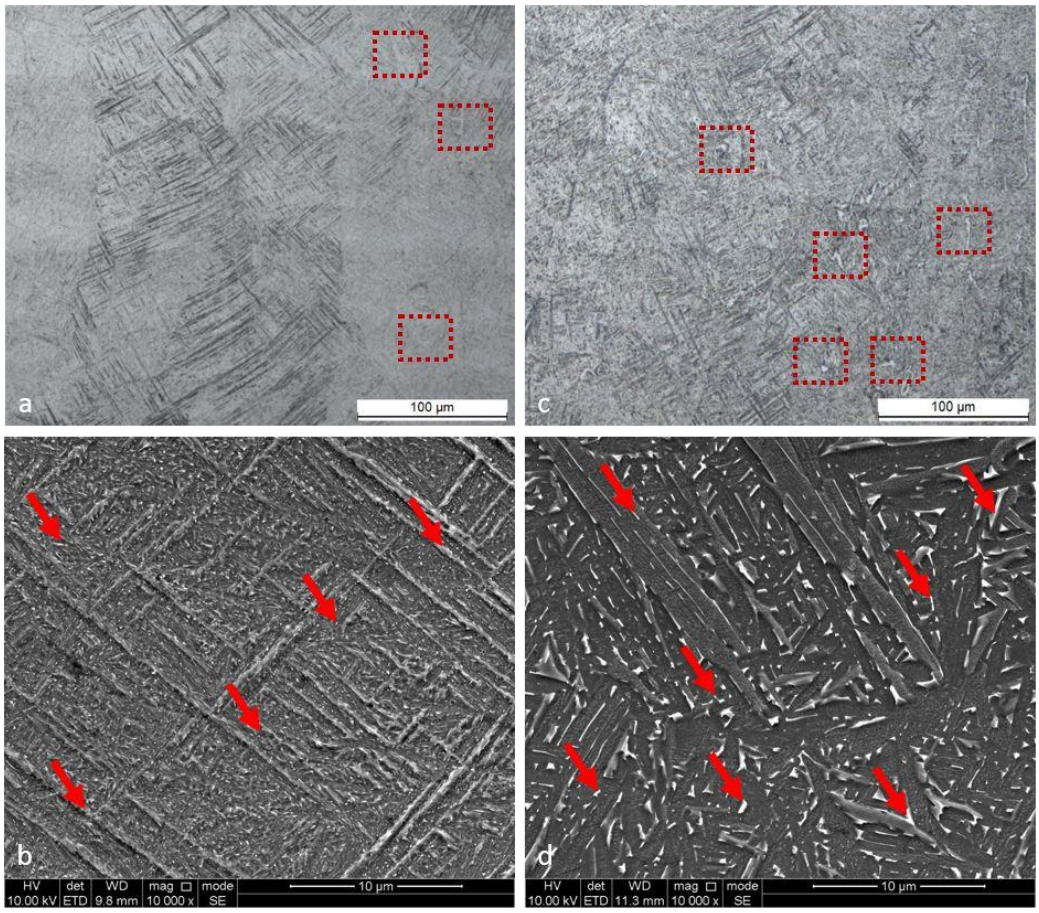

Figure-6. (a) Case-T5 (670ºC), showing the start of grain boundary α globulorisation, highlighted by the red rectangles. (b) Case-T5 showing the growth in white β particles between and inside α laths (indicated by the red arrows). (c) Case-T6 (770ºC) shows an increase in globular α, highlighted by the red rectangles. (d) Case-T6 shows an increase in grain boundary β and β inside α laths (indicated by the red arrows).

Figure-7(a) shows that α globularisation occurs in the samples built with a pre-heat bed temperature of 670ºC. These effects was increased by higher bed temperatures as it is shown in Figure-7(b) where solid red rectangles highlight globular α grains. Figure-7 (a) and (b) also show that at 670ºC and 770ºC a wide size range of α laths exists in the samples. Figure-7(c) shows the nano β growing inside α laths highlighted by the red ellipses, which appeared at 570ºC and increased further at higher pre-heat temperatures.

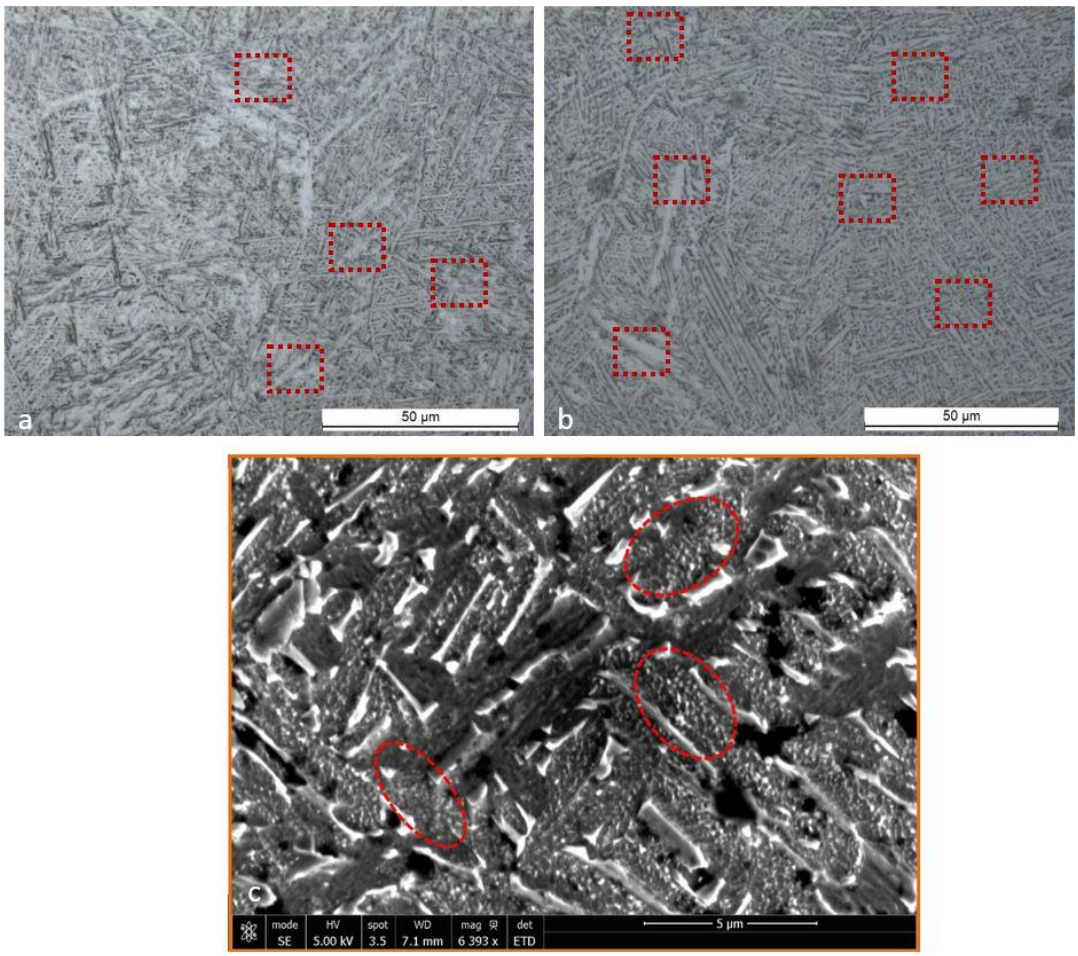

Figure-7(a) Optical micrograph of 670ºC sample showing globular α highlighted by red rectangles. (b) Optical micrograph of 770ºC sample showing globular α highlighted by red rectangles. (c) SEM secondary image of 770ºC sample showing nano β-particles inside α-laths highlighted by red ellipses.

3.3 **Residual Stress**

Figure-8 shows the measured residual stress in SLM cubes manufactured with increasing bed temperatures. There is clearly an inverse relationship between bed temperature and residual stress. Case-T2, shows that increasing the bed temperature to 370ºC resulted in a 71% reduction in residual stresses compared with Case-T1 where samples were produced at a standard 100ºC. For the samples in Case-T3 at 470ºC, the generated residual stresses were 88.3% lower compared to Case-T1. Case-T4, with samples built at 570ºC, 30ºC below the lower limit of Ti6Al4V martensitic decomposition temperature (600-670ºC), no significant residual stresses were present within the samples. Similarly for samples built at 670ºC (Case T5), the higher limit of the martensitic

decomposition temperature range and 30ºC below the lower limit of the annealing temperature (700-790ºC) for Ti6Al4V, no residual stress was measured within the samples. Case-T6 with samples built at 770ºC, 20ºC below the higher limit of the annealing temperature range, also showed no significant residual stress formation. In some samples, e.g. Case-T4 and T6 there was some evidence of compressive residual stresses that may be beneficial for improved fatigue life (this may also be due to measurement error). According to the Temperature Gradient Mechanism (TGM) and cool-down phase models, the previously melted powder layer's material shrinkage during re-solidification is partially inhibited by underlying material which results in the buildup of tensile residual stresses (σ_{tens}) in the top layer [29, 39]. Increasing the bed pre-heat temperature lowers the temperature gradient between the melt-pool and the surrounding material leading to a reduction in residual stress build up. Increased pre-heating temperature may only be partly responsible for reducing residual stress. According to Vasinonta et al.[40], a reduction in the yield strength of materials at higher temperatures is important in limiting the residual stress build-up, which explains the reduction in residual stress with increasing bed temperatures. Figure-9 data adapted from [41], shows that the yield strength of wrought annealed Ti6Al4V decreases with increasing temperature, this corroborates with the theory of Vasinonta et al. Figure-9 also shows that at higher temperatures the Young's modulus decreases, this results in lowering the overall residual stress buildup. Figure-9 shows that both the yield strength and Young's modulus at 570°C decreased by 40-45%, while at 100°C the yield strength as well as the Young's Modulus decreased only by about 10% compared to the values measured at the room temperature [41].

According to the graph of Figure-8 the standard deviation of the measured residual stresses decreases at higher temperatures. Therefore, it is proposed here that higher bed temperatures enhance the repeatability of measured residual stress values within the SLM process compared to standard SLM builds carried out at 100°C, which is possible due to the formation of a more uniform α+β microstructure achieved at higher temperature as shown in Figure-4 to Figure-6.

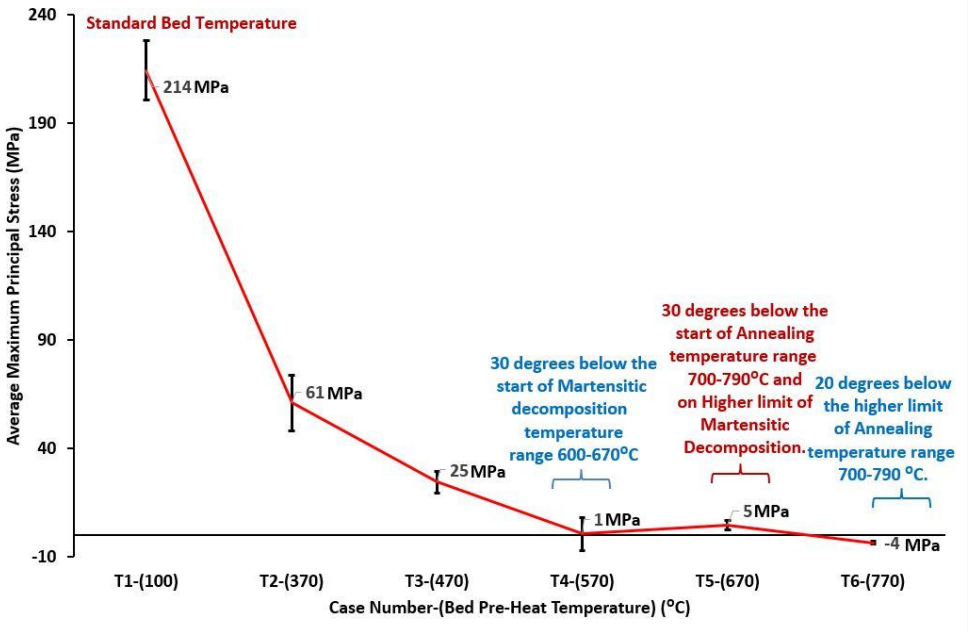

Figure-8. Effect of powder bed pre-heat temperature on Ti6Al4V SLM component residual stress

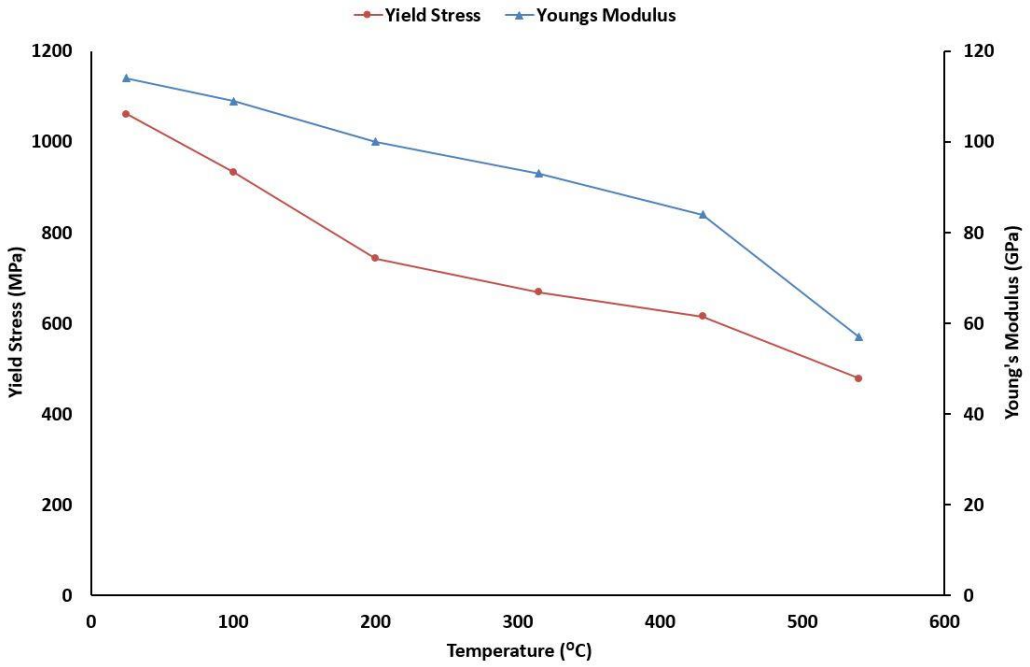

Figure-9. Yield stress and Young's modulus of wrought annealed Ti6Al4V as a function of temperature. Data adapted from [41].

3.4 **Mechanical Properties**

Figure-10 shows stress-strain curves for one sample per powder bed pre-heating temperature used in this study. This stress-strain data was used to approximate the mechanical properties for samples built at each powder bed pre-heat temperature as shown in Figure-11. The young's modulus values for all test cases T-1 to T-5 were similar at approximately 114±5 GPa. Test case T-6 built at 770°C powder bed pre-heat temperature resulted in a young's modulus of 207GPa.

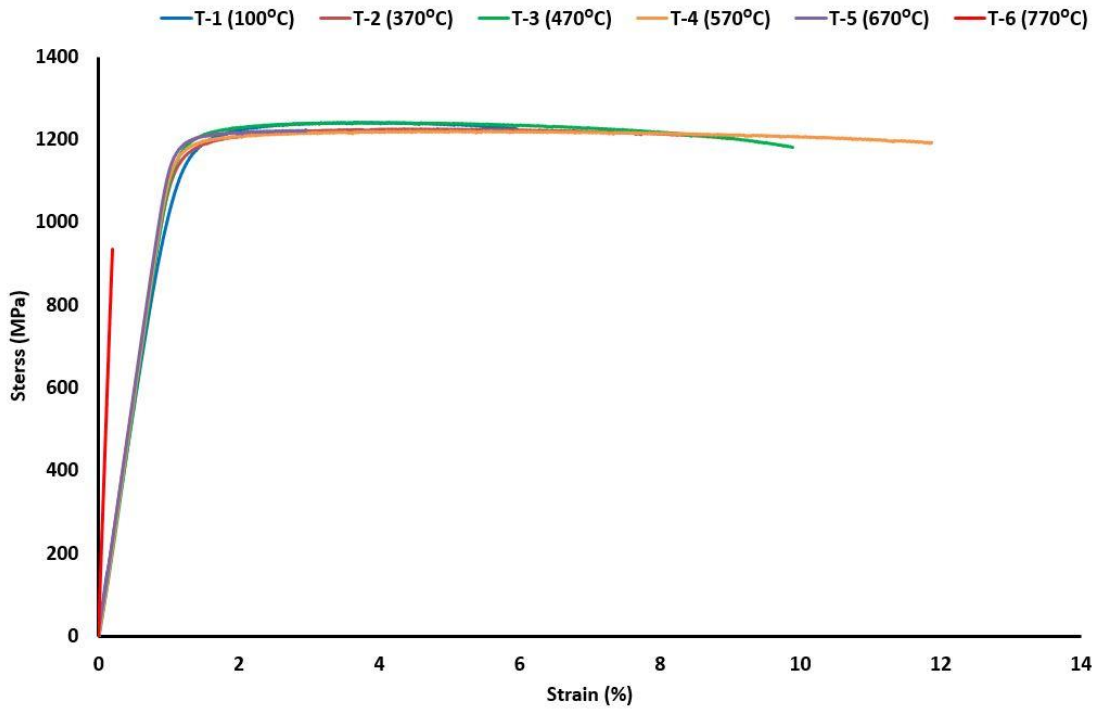

Figure 10. Stress-strain curve of one sample per powder bed pre-heat temperature

Figure-11 shows the effect of powder bed pre-heating on mechanical properties of Ti6Al4V SLM components. It can be seen that Ultimate Tensile Strength (UTS) for samples remains consistent up to 570°C, with only 3% decrease at 670°C compared with standard SLM samples in Case-T1 built at 100°C.

Increasing the bed temperature up to 770°C causes a sharp decline of 39.3% in UTS compared to Case-T1.

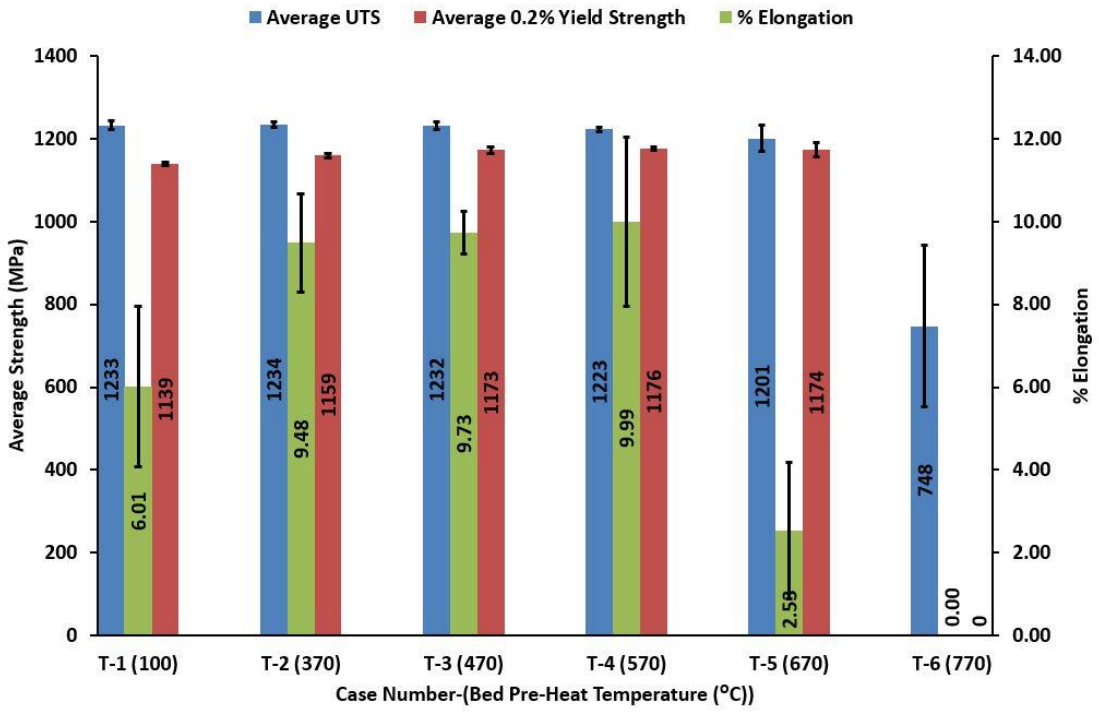

Figure-11. Effect of powder bed pre-heat temperature on UTS, yield strength and elongation

3.4.1 Yield Strength

The yield strength of the samples increased by 3.2% when the bed temperature was increased from 100°C to 470°C. A relatively consistent value was observed up to a bed temperature of 670°C above which a premature fracture occurred preventing any measured value for the yield strength to be obtained. This premature failure may have been a result of sub-optimal processing parameters being inappropriate at high bed temperatures. Another factor that may have led to premature failure is the increased grain sizes generated at higher bed temperatures (as shown in Figure-7). According to Lütjering et al, [42, 43] α colony size greatly affects the mechanical properties for lamellar microstructures. The effective slip length is a function of the colony size, which is inversely related to the cooling rate from the β phase field. Inherent high cooling rates of the SLM process lead to a totally martensitic microstructure, which has slip lengths and colony sizes equal to the width of the individual

martensitic α' plates. Figure-12(a) shows that yield stress increases with decreasing slip length and Figure-12(b) shows an exponential growth in the rate of increase in yield stress with cooling rate, beyond $1000\frac{^oC}{min}$, the cooling rate for air cooling. According to Manikandakumar et al [44], the α colony and α lath size determines the properties of SLM build Ti6Al4V. Dislocation pile ups are generated due to the smaller α lath size and α colony size being equal to a single martensitic α' laths. Smaller α colony sizes of the martensitic microstructure restricts the movement of dislocations and limits the plastic deformation in SLM Ti6Al4V components. This results in a higher yield strength and UTS of SLM parts. Based on the effective slip length and dislocation movement theories [42, 43], the yield strength should decrease with increasing bed temperature as it leads to a slower cooling rate and larger colonies of α. No decrease in the yield strength of SLM components built at high bed pre-heat temperature can be attributed to the fact that even at the highest bed temperature, the cooling rate is still much higher than $10000\frac{^oC}{min}$, the cooling rate of water quenched samples (highest yield strength) shown in Figure-12 (b). Additionally, the formation of nano β particles in α laths as shown by the SEM images in Figure-4 to Figure-6 may be responsible for high yield strength of SLM samples built at high bed pre-heat temperatures.

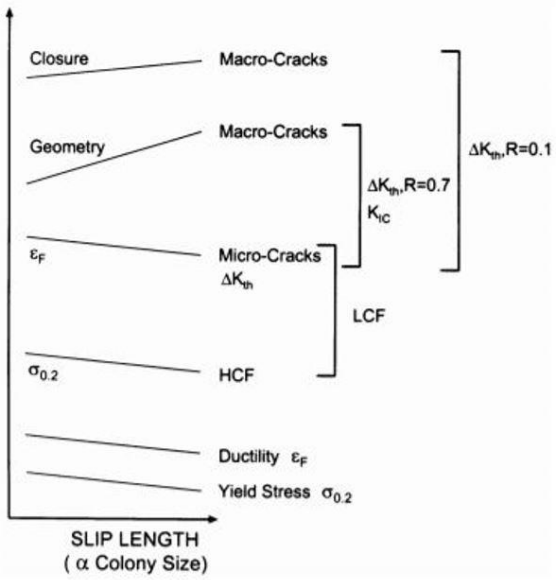

(a)

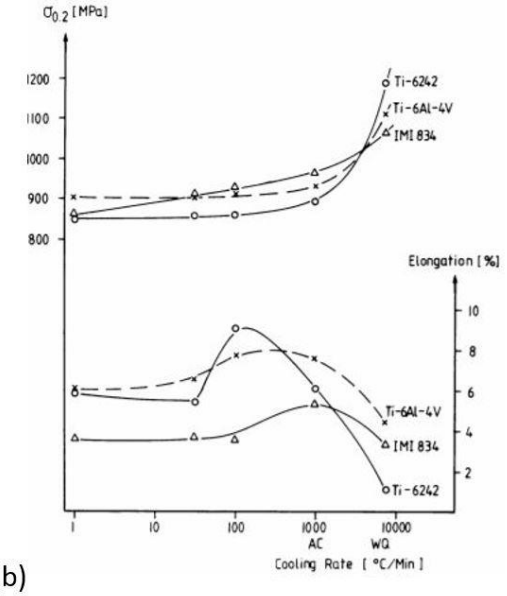

(b)

Figure 12(a) Influence of slip length (α colony size) on mechanical properties, (schematically). (b) Effect of cooling rate from the β phase field on yield stress and ductility of fully lamellar structures [42, 43].

3.4.2 Ductility

Figure-11 showed an increasing trend in sample elongation with increasing temperature, there is a 57.74% increase in elongation for Case-T2, samples built at a bed temperature of 370°C compared with the standard samples Case-T1 built at 100°C. Raising the bed temperature to 570°C Case-T4 improves the elongation by another 5.4% compared with Case-T3 where the bed temperature was 470°C, while compared to the standard samples Case-T1, the elongation has improved by 66.2%. Increasing the temperature to 670°C Case-T5 produces a sharp decline of 74.7% compared to Case-T4 at 570°C and at 770°C Case-T6. According to Lütjering et al. [42, 43] ductility behaves in a more complex manner with changing cooling rates. Figure-12(a) showed an increase in ductility with decreasing slip length. Figure-12(b) showed that ductility reaches a maximum value up to a certain cooling rate, beyond which an increase in the cooling rate results in a sharp decline in ductility. According to Sujoy Kumar [45] a reduction in slip length with higher cooling rate reduces the pile-up length, which leads to lower stress concentrations and delays crack nucleation resulting in improved ductility. Secondly the decrease in ductility with increasing cooling rate after an intermediate point is caused by the refinement of the lamellar structure, which leads to an increase in the strength of the matrix. However the difference in matrix strength and the coarser α-layers along the β-grain boundaries leads to preferential premature crack nucleation in the softer grain boundary α [45]. The cooling rate decreases with increasing bed temperature but is still higher than the optimum intermediate cooling rate which results in a maximised ductility. However, the improvement can be attributed to shifting closer to the cooling rate for maximum ductility. Based on the cooling rate, Case-T5 at 670°C and Case-T6 at 770°C should have produced samples with improved ductility, however results in Figure-11 indicate that a bed temperature of 670°C Case-T5 produced a sharp decline of 74.7% in %

elongation compared to Case-T4 built at 570°C and at 770°C Case-T6. This cannot be attributed to the second mechanism of matrix strength increasing in comparison to the coarser grain boundary α and causing premature crack nucleation. For this to occur an increase in the cooling rate would be required whereas in this scenario the cooling rate is in-fact decreasing. According to Qian et al.[46], the cooling rate and residence time at temperatures between 600-980°C, just below the β transus temperature are very important in terms of α laths growth in a basket-weave microstructure. Getting closer to the β transus temperature enhances the speed of which α laths growth [46] in Direct Laser Fabrication (DLF) of Ti6Al4V samples. In principle SLM is similar to DLF with the only difference being the delivery of powder feed (DLF blows powder into the path of a focused laser, much like laser cladding). The thermal cycles experienced during the high temperature SLM process can be approximated by the DLF process, therefore the reasoning reported in ref-[46], can be extended to the high temperature bed samples built at 670°C and 770°C. As can be seen in Figure-7 (a) and (b), at 670°C and 770°C there has been considerable grain growth with some globular α grains highlighted by red ellipses. The microstructure containing a range of sizes of α laths. Similarly, Figure-7(c) shows that the grain boundary β has also considerably grown. The existence of globular and larger α laths and colonies indicate larger slip lengths and according to Figure-12 (a) lower yield strength as well as lower ductility [42, 43]. The variation in grain size across the microstructure and the existence of coarser grain boundary β together would lead to the creation of weaker locations for crack nucleation and growth. These weaker sites probably led to the premature failure of the tensile specimens outside the gauge length. Another important factor is that with the existence of such grain boundary weak locations, porosity becomes important as any internal defect will enhance the premature failure. Since the parameters were optimised for 100ºC bed pre-heat temperature use of these for higher bed temperatures may not be appropriate, this combined with non-equilibrium grain sizes can lead to premature failure. For further work optimising the process parameters will be required separately for each bed temperature to determine true mode of failure and improve mechanical properties of SLM Ti6Al4V parts above 670ºC pre-heat.

3.4.3 Hardness

Figure-13 shows that the micro-Vickers hardness of samples increases with increasing bed temperatures up to 670°C, with 13% increase at 670°C Case-T5 compared to Case-T1 samples built at 100°C. It can be seen that the value decreases by about 1.8% when the bed pre-heat temperature is increased to 770°C Case-T6. This increase in micro-hardness can be attributed to the amount of β between α'/α laths increasing in the samples up to 470°C bed temperature, while at 570°C and above the amount of β increases between the α colony boundaries and nano β growth inside the α laths. It can be seen that the value decreases by about 1.8% when the bed temperature is increased to 770°C, while Figure-6 shows that the amount of β between α colonies boundaries as well as the amount of Nano β particles inside α laths has increased. This decrease in micro-hardness despite the increase in β in the samples can be attributed to the increase in the grain size which is clearly evident from the comparison of the SEM images shown in Figure-4 to Figure-6. Figure-7 clearly illustrates the β grown between α colonies grain boundaries and the Nano β grown inside α laths. An important factor evident from Figure-13 is that the hardness across the height of the samples at higher bed temperatures is consistent as shown by the values for standard deviation. This indicates that the sample has a consistent micro structure throughout the height. The standard deviation of 100°C sample shows a wide spread in the hardness across the 12 indentations taken along the build direction of the sample. This indicates that the microstructure across the sample may not be uniform, corroborated by the existence of internal microstructural defects shown in the SEM image of Case-T1 built at 100°C in Figure-4.

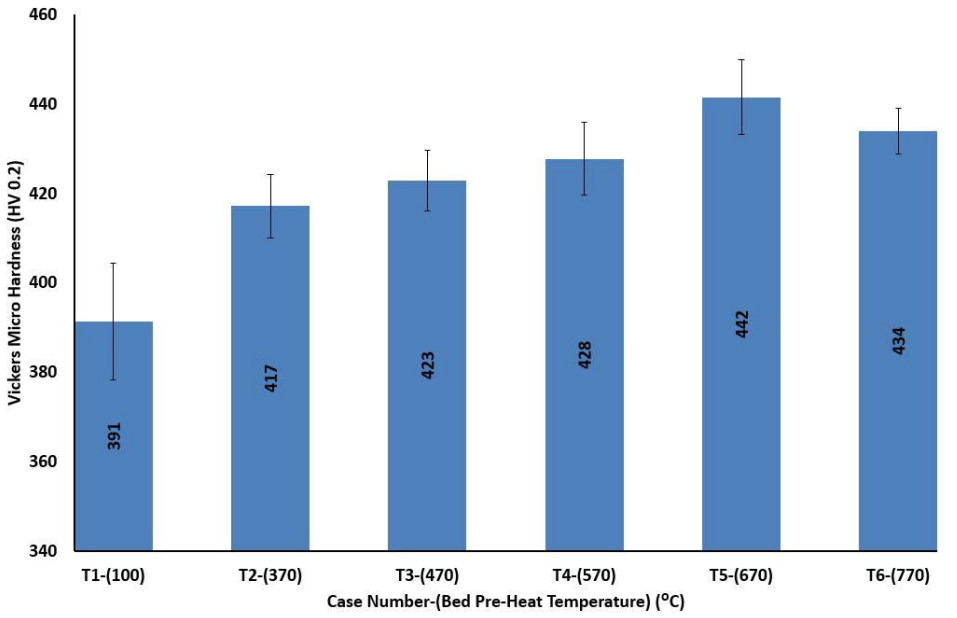

Figure 13. Effect of bed pre-heat temperature on Vickers micro-hardness

4 Conclusions

SLM Ti6Al4V martensitic microstructure can be completely transformed into a basketweave α+β microstructure at 570°C powder bed pre-heating (30°C below the start of the martensitic decomposition range of 600-650°C). This microstructural transformation can be attributed to the fact that after completion of the build the cooling rate is only $30\frac{^{o}C}{min}$, which is much lower than the cooling rate required for martensitic formation in Ti6Al4V. As expected powder bed temperature has an inverse relationship with cooling rate, raising the bed temperature lowers the thermal gradient experienced within the SLM process and therefore the formation of residual stresses present within the component. Powder bed pre-heat temperatures of ~570°C significantly reduce residual stress generated within an SLM build. At high bed temperatures (i.e 570°C and 770°C) some samples exhibited compressive residual stress, which can be beneficial for the fatigue life of components. Use of elevated bed temperatures lead to a reduction in cooling rate across a laser processed powder bed, producing parts with high yield strength of 1176 MPa, at 570°C bed pre-heat temperature. At 370°C pre-heat the yield strength improved by 3.2% compared to samples built at 100°C and remained consistent up to a pre-heat temperature

of 670°C. This increasing trend in yield strength with temperature can be attributed to the formation of nano β particles inside α'/α laths of the SLM components. Since the cooling rate at the highest bed pre-heat temperature is still higher than water quenching of Ti6Al4V, therefore no decrease in yield strength is seen with increasing bed temperatures (up till 570ºC). At 770°C there was a sharp decline in yield strength due to pre-mature failure of tensile samples. The pre-mature failure of samples at 770ºC may be attributed to use of sub-optimal processing parameter and the formation of weak microstructural locations due to α globulorisation and increase in grain boundary β. Another major microstructural feature which may be responsible for this pre-mature failure is the existence of a wide range of sizes of α laths in the samples. The ductility of the samples improved with increasing bed temperature, at 570°C there was an improvement of 66.2% elongation in samples compared to those build at a standard 100°C. At 670°C there was a sharp decline of 74.7% compared to 570ºC in sample elongation, this again may be related to use of sub-optimal parameters, increased grain growth resulting in the growth of globular α, existence of α laths in various sizes and the growth of grain boundary β. All these factors leading to non-equilibrium micro-structure and maximising the possibility of weaker locations for crack nucleation and growth, Vickers micro-hardness increased with increasing bed temperature reaching a maximum of 442 [HV 0.2], at 670°C, with a 13% increase compared to samples built at 100°C. This increase in hardness was due to the increase in β content between α/α' laths and at higher temperature nano β growing within α laths. At 770°C there is a 1.8% decrease due to the increase in α laths size even though the amount of β increased.

5 Acknowledgements

The authors would like to thank TWI and EPSRC (grant number EP/I028331/1) for their support during this investigation.

6 References

1. M, B., *Automated fabrication: improving productivity in manufacturing*. 1993, Englewood Cliffs, NJ: Prentice Hall.
2. Gibson, I., D.W. Rosen, and B. Stucker, *Additive Manufacturing Technologies: Rapid Prototyping to Direct Digital Manufacturing*. 2009: Springer. pp.1-14.
3. C. Casavola, S.L.C., C. Pappalettere. *EXPERIMENTAL ANALYSIS OF RESIDUAL STRESSES IN THE SELECTIVE LASER MELTING PROCESS*. in *Proceedings of the XIth International Congress and Exposition*. 2008. Orlando, Florida USA.
4. L. Papadakis & A. Loizou, J.R.S.B., *A thermo-mechanical modeling reduction approach for calculating shape distortion in SLM manufacturing for aero engine components* in *VRAP Advanced Research in Virtual and Rapid Prototyping*: Portugal.
5. Kruth, J.-P., et al., *Assessing and comparing influencing factors of residual stresses in selective laser melting using a novel analysis method.* Proceedings of the Institution of Mechanical Engineers, Part B: Journal of Engineering Manufacture, 2012. **226**(6): p. 980-991.
6. Rossini, N.S., et al., *Methods of measuring residual stresses in components.* Materials & Design, 2012. **35**(0): p. 572-588.
7. Matsumoto, M., et al., *Finite element analysis of single layer forming on metallic powder bed in rapid prototyping by selective laser processing.* International Journal of Machine Tools and Manufacture, 2002. **42**(1): p. 61-67.
8. Zaeh, M.F.B., G., *Investigations on residual stresses and deformations in selective laser melting.* Production engineering : research and development in Germany, 2010. **4**(1).
9. Withers, P.J.B., H.K.D.H, *Residual stress. Part 1 – Measurement techniques.* Materials Science and Technology, 2001. **17**(4): p. 355-365.
10. Withers, P.J.B., H.K.D.H, *Residual Stress Part 2- Nature and origins.* Materials Science and Technology, 2001. **17**(4): p. 366-375.
11. Van Belle, L.V., Guillaume Boyer, Jean Claude, *Investigation of Residual Stresses Induced during the Selective Laser Melting Process.* Key Engineering Materials, 2013. **554-557**: p. 1828-1834.
12. Tatsuaki Furumoto, T.U., Mohd Sanusi Abdul Aziz, Akira Hosokawa, Ryutaro Tanaka, *Study on Reduction of Residual Stress Induced during Rapid Tooling Process- Influence of Heating Conditions on Residual Stress.* Key Engineering Materials, 2010. **487-488**: p. 785-789.
13. Roberts, I.A., *INVESTIGATION OF RESIDUAL STRESSES IN THE LASER MELTING OF METAL POWDERS IN ADDITIVE LAYER MANUFACTURING*, 2012, University of Wolverhampton. p. 246.
14. Joe Elambasseril, S.F., Matthias Bringezu and Milan Brandt, *Influence of process parameters on selective laser melting of Ti 6Al-4V components*, 2012, RMIT University School of Aerospace, Mechanical and Manufacturing Engineering (SAMME).
15. S. Das, M.W., J.J. Beaman, D.L. Bourell, *Producing metal parts with selective laser sintering/hot isostatic pressing.* Journal JOM 50 1998. **12**: p. 17–20.
16. Vrancken, B., et al. *Influence of preheating and oxygen content on Selective Laser Melting of Ti6Al4V*. in *Proceedings of the 16th RAPDASA Conference. RAPDASA, Annual*

International Conference on Rapid Product Development Association of South Africa 4-6 November 2015. Pretoria, South Africa.

17. Facchini, L., et al., *Ductility of a Ti-6Al-4V alloy produced by selective laser melting of prealloyed powders.* Rapid Prototyping Journal, 2010. **16**(6): p. 450-459.

18. Xu, W., et al., *Ti-6Al-4V Additively Manufactured by Selective Laser Melting with Superior Mechanical Properties.* JOM, 2015. **67**(3): p. 668-673.

19. J.-P. Kruth, M.B., E.Yasa, J. Deckers, L. Thijs, J. Van Humbeeck. *Part and material properties in selective laser melting of metals*. in *16th International Symposium on Electromachining (ISEM XVI)*. 2010. shanghai-china.

20. Gong, H., et al., *Influence of defects on mechanical properties of Ti–6Al–4 V components produced by selective laser melting and electron beam melting.* Materials & Design, 2015. **86**: p. 545-554.

21. Leuders, S., et al., *On the mechanical behaviour of titanium alloy TiAl6V4 manufactured by selective laser melting: Fatigue resistance and crack growth performance.* International Journal of Fatigue, 2013. **48**: p. 300-307.

22. M., J.R.I.a.B.H., *Titanium Science and Technology*. Vol. 1. 1973: Springer.

23. Donachie, M.J., *Titanium: A Technical Guide, 2nd Edition*. 2000: ASM International.

24. *Titanium and Titanium Alloys. Fundamentals and Applications*. 2003: Wiley-VCH GmbH & Co. KGaA.

25. Xu, W., et al., *Additive manufacturing of strong and ductile Ti–6Al–4V by selective laser melting via in situ martensite decomposition.* Acta Materialia, 2015. **85**: p. 74-84.

26. Tan, X., et al., *Revealing martensitic transformation and α/β interface evolution in electron beam melting three-dimensional-printed Ti-6Al-4V.* Scientific Reports, 2016. **6**: p. 26039.

27. Welsch, G., R. Boyer, and E.W. Collings, *Materials Properties Handbook: Titanium Alloys*. 1993: ASM International.

28. Vora, P., et al., *AlSi12 in-situ alloy formation and residual stress reduction using anchorless selective laser melting.* Additive Manufacturing, 2015. **7**: p. 12-19.

29. Shiomi, M., et al., *Residual Stress within Metallic Model Made by Selective Laser Melting Process.* CIRP Annals - Manufacturing Technology, 2004. **53**(1): p. 195-198.

30. Vrancken, B., et al., *Heat treatment of Ti6Al4V produced by Selective Laser Melting: Microstructure and mechanical properties.* Journal of Alloys and Compounds, 2012. **541**: p. 177-185.

31. Thöne, M., et al. *Influence of heat-treatment on selective laser melting products–eg Ti6Al4V*. in *Solid freeform fabrication symposium SFF, Austin Texas*. 2012.

32. Harrison, N.J., *Selective Laser Melting of Nickel Superalloys: solidification, microstructure and material response*, in *Mechanical Engineering*2016, University of Sheffield.

33. ASTM, *E2109-01(2007), Standard Test Methods for Determining Area Percentage Porosity in Thermal Sprayed Coatings*, 2007, ASTM International: West Conshohocken, PA.

34. BSI, *BS 7590:1992, Method for statistically estimating the volume fraction of phases and constituents by systematic manual point counting with a grid*, 1992, BSI.

35. ASTM, *E8 / E8M-13a, Standard Test Methods for Tension Testing of Metallic Materials*, 2013, ASTM International: West Conshohocken, PA.

36. BSEN, *ISO 6892-1, Metallic materials. Tensile testing. Method of test at ambient temperature*, 31 August, 2009.

37. BSEN, *ISO 6507-1:2005, Metallic materials. Vickers hardness test. Test method*, 2006.

38. Simchi, A., *Direct laser sintering of metal powders: Mechanism, kinetics and microstructural features.* Materials Science and Engineering: A, 2006. **428**(1): p. 148-158.

39. Mercelis, P., *Control of selective laser sintering and selective laser melting processes*, 2007, KU Leuven, Leuven, Belgium.

40. Vasinonta, A., J.L. Beuth, and M. Griffith, *Process Maps for Predicting Residual Stress and Melt Pool Size in the Laser-Based Fabrication of Thin-Walled Structures.* Journal of Manufacturing Science and Engineering, 2006. **129**(1): p. 101-109.

41. USDD, *Military Handbook-MIL-HDBK-5J: Metallic Materials and Elements for Aerospace Vehicle Structures*. 2003: U.S. Department of Defence.

42. Lütjering, G. and J.C. Williams, *Titanium*. 2003: Springer.

43. Lütjering, G., *Influence of processing on microstructure and mechanical properties of (α+β) titanium alloys.* Materials Science and Engineering: A, 1998. **243**(1–2): p. 32-45.

44. Shunmugavel, M., A. Polishetty, and G. Littlefair, *Microstructure and Mechanical Properties of Wrought and Additive Manufactured Ti-6Al-4V Cylindrical Bars.* Procedia Technology, 2015. **20**: p. 231-236.

45. Kar, S.K., *Modeling of mechanical properties in alpha/beta-titanium alloys*, 2005, The Ohio State University.

46. Qian, L., J. Mei, and X.H. Wu. *An experimental and modelling study of laser fabricated samples*. in *Materials science forum*. 2007. Trans Tech Publ.